Monthly Notices
of the
ROYAL ASTRONOMICAL SOCIETY

Mon. Not. R. Astron. Soc. **415,** 3219–3226 (2011) doi:10.1111/j.1365-2966.2011.18933.x

Anisotropy of Alfvénic turbulence in the solar wind and numerical simulations

C. H. K. Chen,[1,2]★ A. Mallet,[3] T. A. Yousef,[4] A. A. Schekochihin[3] and T. S. Horbury[2]

[1]*Space Sciences Laboratory, University of California, Berkeley, CA 94720, USA*
[2]*The Blackett Laboratory, Imperial College London, London SW7 2AZ*
[3]*Rudolf Peierls Centre for Theoretical Physics, University of Oxford, Oxford OX1 3NP*
[4]*Bjørn Stallares gt 1, 7042 Trondheim, Norway*

Accepted 2011 April 18. Received 2011 March 24; in original form 2010 September 3

ABSTRACT

We investigate the anisotropy of Alfvénic turbulence in the inertial range of slow solar wind and in both driven and decaying reduced magnetohydrodynamic simulations. A direct comparison is made by measuring the anisotropic second-order structure functions in both data sets. In the solar wind, the perpendicular spectral index of the magnetic field is close to −5/3. In the forced simulation, it is close to −5/3 for the velocity and −3/2 for the magnetic field. In the decaying simulation, it is −5/3 for both fields. The spectral index becomes steeper at small angles to the local magnetic field direction in all cases. We also show that when using the global rather than local mean field, the anisotropic scaling of the simulations cannot always be properly measured.

Key words: magnetic fields – MHD – plasmas – turbulence – solar wind.

1 INTRODUCTION

The solar wind is a turbulent plasma (see reviews by Goldstein, Roberts & Matthaeus 1995; Bruno & Carbone 2005; Horbury, Forman & Oughton 2005) with a power spectrum extending over many orders of magnitude (e.g. Coleman 1968). Scales larger than the ion gyroradius are known as the inertial range, and the spectral indices at 1 au are observed to be close to −5/3 for the magnetic and electric fields and −3/2 for velocity (e.g. Matthaeus & Goldstein 1982; Bale et al. 2005; Podesta, Roberts & Goldstein 2007; Tessein et al. 2009; Podesta & Borovsky 2010). There is also evidence that the fluctuations are predominantly Alfvénic (e.g. Belcher & Davis 1971; Horbury et al. 1995; Bale et al. 2005).

Solar wind turbulence is anisotropic with respect to the direction of the magnetic field. For example, the magnetic field correlation length has been shown to vary depending on the angle of observation with respect to the field direction (Crooker et al. 1982; Matthaeus, Goldstein & Roberts 1990; Dasso et al. 2005; Osman & Horbury 2007; Weygand et al. 2009). The magnetic field power and spectral indices are also observed to be anisotropic: power at a fixed scale increases with angle to the magnetic field (Bieber, Wanner & Matthaeus 1996; Horbury et al. 1998; Osman & Horbury 2009) and the spectral index varies from −2 at small angles to between −3/2 and −5/3 in the field perpendicular direction (Horbury, Forman & Oughton 2008; Podesta 2009; Luo & Wu 2010; Wicks et al. 2010, 2011). These observations are consistent with theories of critically balanced magnetohydrodynamic (MHD) turbulence, for example that of Goldreich & Sridhar (1995), which predicts anisotropic fluctuations ($k_\perp > k_\parallel$) and the −2 and −5/3 spectral indices.

Many simulations of plasma turbulence have been performed, most of which have used the equations of incompressible MHD. When a strong mean magnetic field is present, the spectral index of the total energy is closer to −3/2 than −5/3 (Maron & Goldreich 2001; Müller, Biskamp & Grappin 2003; Müller & Grappin 2005; Mason, Cattaneo & Boldyrev 2008; Perez & Boldyrev 2008; Grappin & Müller 2010), although a limited inertial range and the bottleneck effect (Falkovich 1994) make this number hard to determine precisely (Beresnyak & Lazarian 2009; Beresnyak 2011).

Anisotropy has also been measured in MHD simulations. Early 2D simulations showed that the turbulence develops wavevector anisotropy so that the fluctuations have $k_\perp > k_\parallel$ (Shebalin, Matthaeus & Montgomery 1983), and this was later confirmed in 3D simulations (Oughton, Priest & Matthaeus 1994; Matthaeus et al. 1996; Milano et al. 2001). The anisotropy was found to be scale-dependent, such that $k_\parallel \sim k_\perp^{2/3}$ (Cho & Vishniac 2000; Maron & Goldreich 2001), in agreement with the critical balance predictions (Goldreich & Sridhar 1995). An important point noted in these studies, and also in solar wind measurements (Horbury et al. 2008), was that the anisotropic scaling is with respect to the scale-dependent local mean field and not the global mean field.

The theory of Goldreich & Sridhar (1995) was modified by Boldyrev (2006) by including a phenomenon called scale-dependent dynamic alignment. In this theory, the velocity and magnetic field fluctuations align to within a smaller angle at smaller scales and the perpendicular spectral index becomes −3/2. There is evidence for

★E-mail: chen@ssl.berkeley.edu

this scale-dependent dynamic alignment in the solar wind (Podesta et al. 2009) and some driven MHD simulations (Mason, Cattaneo & Boldyrev 2006; Mason et al. 2008), although higher resolution simulations suggest that the alignment saturates at small scales (Beresnyak 2011).

To date, there has not been a measurement of the spectral index parallel to the local magnetic field in simulations. Measurements of the perpendicular spectral index in the solar wind and in simulations are also not always in agreement. It is important to be sure that the same quantities are being measured in both the solar wind and simulations and the subject of this paper is such a comparative study. We apply a similar analysis technique to both solar wind data and reduced MHD (RMHD) simulations, to make a direct comparison of the anisotropic scaling. In Section 2 we present the solar wind analysis, in Section 3 we present the simulation analysis, in Section 4 we compare the local and global mean field methods and in Section 5 we present our conclusions.

2 INERTIAL RANGE SOLAR WIND MEASUREMENTS

2.1 Data intervals

In this section, we apply the multispacecraft method of Chen et al. (2010a) to obtain the power and spectral index anisotropy of inertial range turbulence in the slow solar wind at 1 au. The technique is applied to 65 1-h intervals of data from the *Cluster* spacecraft (Escoubet, Fehringer & Goldstein 2001) from 2005 December to 2006 April, when the typical separation between the four spacecraft was ∼10 000 km. The selected intervals are from the parts of the *Cluster* orbit where the spacecrafts were in the free solar wind upstream of the bow shock at geocentric distances of between 15 R_E and 20 R_E. They contain no evidence of ion foreshock activity: signatures typical of the ion foreshock, such as enhanced magnetic field fluctuations and high-energy ions, are not present. The time series were also inspected visually to ensure that they are approximately stationary and do not contain shocks or magnetic clouds.

In the analysis, we use 4-s measurements of the magnetic field from the fluxgate magnetometer (FGM) (Balogh et al. 2001) and velocity and density moments from the *Cluster* ion spectrometer (CIS) (Rème et al. 2001). The mean values of various parameters for the 65 intervals are given in Table 1. The geometric mean is used for the ion beta, temperature anisotropy, gyroradius and Alfvén ratio. The intervals are in slow solar wind with a speed $<550\,\mathrm{km\,s^{-1}}$.

The Alfvén ratio is the ratio of energy in the velocity $\boldsymbol{u}$ to the magnetic field in Alfvén units $\boldsymbol{b}$, and can be calculated spectrally, $r_\mathrm{A} = E^u/E^b$, where E^u and E^b are the power spectra of $\boldsymbol{u}$ and $\boldsymbol{b}$. We calculate the average r_A in the spacecraft frequency range from 2×10^{-3} to 1×10^{-2} Hz, which roughly corresponds to scales 36 000–180 000 km under Taylor's hypothesis (Taylor 1938). While this is at larger scales than the following anisotropy measurements, it is in the range where noise does not appear to dominate the velocity spectra. The value slightly less than unity that we obtain (≈0.7) is consistent with previous measurements (e.g. Matthaeus & Goldstein 1982; Marsch & Tu 1990; Bruno et al. 2007; Podesta et al. 2007; Salem et al. 2009).

Table 1. Mean parameter values for the 65 solar wind intervals.

Solar wind speed (v_sw)	$360 \pm 10\,\mathrm{km\,s^{-1}}$
Ion number density (n_i)	$8.6 \pm 0.4\,\mathrm{cm^{-3}}$
Alfvén speed (v_A)	$40 \pm 2\,\mathrm{km\,s^{-1}}$
Perpendicular ion temperature ($T_{\mathrm{i}\perp}$)	$7.5 \pm 0.4\,\mathrm{eV}$
Ion beta (β_i)	1.1 ± 0.1
Ion temperature anisotropy ($T_{\mathrm{i}\perp}/T_{\mathrm{i}\parallel}$)	0.5 ± 0.2
Ion gyroradius (ρ_i)	74 ± 3 km
Alfvén ratio (r_A)	0.72 ± 0.04

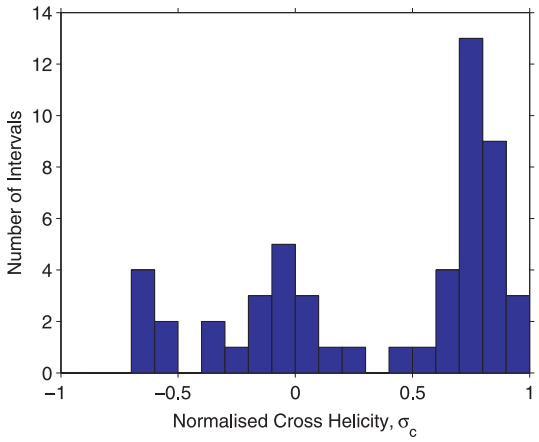

Figure 1. Histogram of normalized cross helicity, σ_c, for 53 of the solar wind intervals in the spacecraft frequency range from 2×10^{-3} to 1×10^{-2} Hz.

We also calculate the normalized cross helicity,

$$\sigma_\mathrm{c} = \frac{E^+ - E^-}{E^+ + E^-}, \tag{1}$$

where E^+ and E^- are the power spectra of the Elsasser variables $\boldsymbol{z}^\pm = \boldsymbol{u} \pm \boldsymbol{b}$. The average value for each interval is calculated over the same range as the Alfvén ratio. The usual convention is used: the Elsasser variables are defined such that positive values of σ_c correspond to Alfvénic propagation away from the Sun. A histogram of σ_c (Fig. 1) shows a range of values with a non-Gaussian distribution: there is a large outward population ($\sigma_\mathrm{c} > 0.5$), a balanced population ($\sigma_\mathrm{c} \approx 0$) and a few inward intervals ($\sigma_\mathrm{c} < -0.5$).

2.2 Analysis technique

For each interval, pairs of points from the time series of the four spacecraft are used to calculate second-order structure functions at different angles to the local magnetic field, as described by Chen et al. (2010a). The second-order structure function is defined as

$$\delta B_i^2(\boldsymbol{l}) = \langle |B_i(\boldsymbol{r}+\boldsymbol{l}) - B_i(\boldsymbol{r})|^2 \rangle, \tag{2}$$

where B_i is the ith component of the magnetic field, $\boldsymbol{l}$ is the separation vector and the angular brackets denote an ensemble average over positions $\boldsymbol{r}$. The local mean magnetic field at scale $\boldsymbol{l}$ is defined as

$$\boldsymbol{B}_\mathrm{local} = \frac{\boldsymbol{B}(\boldsymbol{r}+\boldsymbol{l}) + \boldsymbol{B}(\boldsymbol{r})}{2}. \tag{3}$$

We calculate the structure functions of the local perpendicular magnetic field component $\boldsymbol{B}_\perp$, which corresponds to the Alfvénic fluctuations, at a variety of separations $\boldsymbol{l}$.

The structure function values are binned according to scale parallel, $l_\parallel$, and perpendicular, $l_\perp$, to $\boldsymbol{B}_\mathrm{local}$. Nine linearly spaced bins are used in each direction covering the range 2000–20 000 km, which is within, although towards the small-scale end, the inertial range. The result of this binning for one of the 65 intervals is shown in Fig. 2. It is representative of the average behaviour, although in general each interval is more noisy and has less coverage than this. Most of the

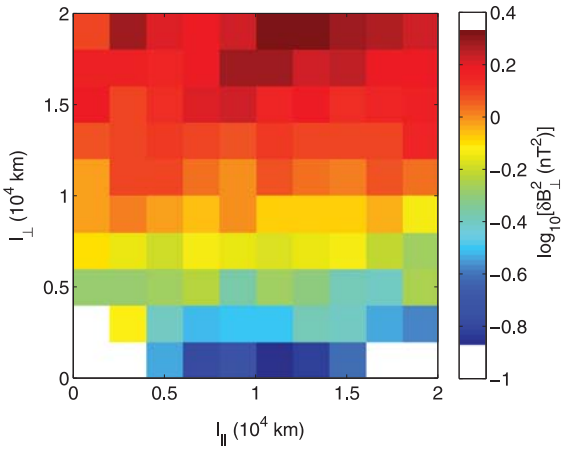

Figure 2. Second-order structure function of the perpendicular magnetic field component for one of the 65 solar wind intervals as a function of parallel ($l_\parallel$) and perpendicular ($l_\perp$) separation.

bin values in this figure are the average of a few thousand structure function values, although some (13 per cent) are of a few hundred. It can be seen that the contours are elongated in the field parallel direction, indicating that the eddies are anisotropic with $k_\perp > k_\parallel$.

The data are also binned according to scale l and the angle θ_B between $\boldsymbol{l}$ and $\boldsymbol{B}_{\rm local}$. Nine linearly spaced scale bins are used over the range 2000–20 000 km and nine linearly spaced angular bins are used between 0° and 90°. Straight lines, in log–log space, are then fitted to the structure functions over the full scale range for each θ_B bin and the power anisotropy is obtained by evaluating these fits at a scale of 10 000 km. The spectral index in each θ_B bin is found using the relation $\alpha = g + 1$, where $-\alpha$ is the spectral index and g is the structure function scaling exponent (Monin & Yaglom 1975). This is similar to the work of Osman & Horbury (2009), except we bin the data with respect to the *local* field direction, since this appears to be the relevant mean field for the fluctuations, and we use many more intervals.

2.3 Magnetic field anisotropy

The results, averaged over all 65 slow wind intervals, are shown in Fig. 3, where the error bars are the standard error of the mean from averaging the intervals. They are similar to previous single spacecraft observations in the fast wind that show that power increases with θ_B and that the spectral index varies from -2 at small angles to between $-5/3$ and $-3/2$ at large angles (Horbury et al. 2008; Podesta 2009; Luo & Wu 2010; Wicks et al. 2010, 2011). This scale-dependent anisotropy, therefore, has now been seen in both fast and slow wind using two different measurement techniques. The power anisotropy is consistent with eddies elongated along the local magnetic field direction and wavevector anisotropy of the form $k_\perp > k_\parallel$ (Chen et al. 2010b).

The -2 scaling at small θ_B is consistent with both the theories of Goldreich & Sridhar (1995) and Boldyrev (2006), which describe critically balanced Alfvénic turbulence. It has been suggested (e.g. Galtier 2010), however, that the parallel scaling of -2 may be due to discontinuities in the data. Using the same technique at smaller scales in the dissipation range, the -2 scaling is not seen (Chen et al. 2010a) because the physics of the turbulence is different at these scales. This suggests that the -2 scaling in the inertial range seen here is in fact due to the properties of the turbulence and not unrelated discontinuities.

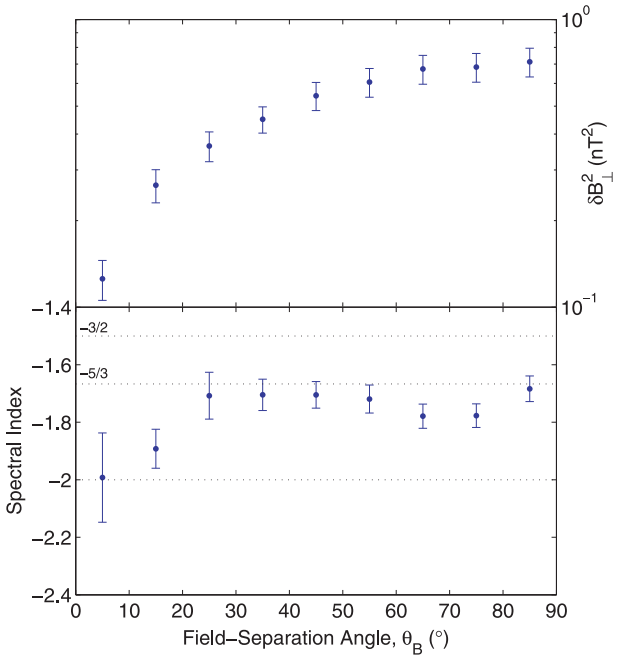

Figure 3. Power anisotropy (upper) and spectral index anisotropy (lower) of the perpendicular magnetic field component in inertial range turbulence in the slow solar wind. The power anisotropy is calculated at $l = 10\,000$ km. Spectral index values of $-3/2$, $-5/3$ and -2 are marked as dotted lines for reference.

The perpendicular spectral index that we obtain here (for $20° < \theta_B < 90°$) is closer to $-5/3$ than $-3/2$. This agrees with the prediction of Goldreich & Sridhar (1995), rather than Boldyrev (2006). Both of these theories, however, apply to balanced turbulence, i.e. $\sigma_c = 0$. As can be seen from Fig. 1, many of the intervals have large σ_c. This is common in the solar wind, and various theories of imbalanced MHD turbulence have been proposed (e.g. Lithwick, Goldreich & Sridhar 2007; Beresnyak & Lazarian 2008; Chandran 2008; Perez & Boldyrev 2009; Podesta & Bhattacharjee 2010). Differentiation between these, however, is beyond the scope of this paper (see Wicks et al. 2011 for a recent observational test of these theories).

In the next section, we apply a similar analysis to RMHD simulations. This enables a direct comparison to be made between turbulence in the solar wind and in numerical simulations.

3 REDUCED MHD SIMULATIONS

3.1 Simulation description

The RMHD equations, originally derived by Strauss (1976), have been used previously to simulate various aspects of MHD turbulence (e.g. Perez & Boldyrev 2008, 2009; Beresnyak 2011). They can be written in Elsasser potentials (Schekochihin et al. 2009):

$$\frac{\partial}{\partial t}\nabla_\perp^2\zeta^\pm \mp v_{\rm A}\frac{\partial}{\partial z}\nabla_\perp^2\zeta^\pm = -\frac{1}{2}(\{\zeta^+,\nabla_\perp^2\zeta^-\}+\{\zeta^-,\nabla_\perp^2\zeta^+\}\mp\nabla_\perp^2\{\zeta^+,\zeta^-\}), \quad (4)$$

where $\{A, B\} = \hat{\boldsymbol{z}}\cdot(\nabla_\perp A\times\nabla_\perp B)$, $\hat{\boldsymbol{z}}$ is the global mean field direction, $v_{\rm A}$ is the Alfvén speed and the Elsasser potentials are defined via $\delta z^\pm_\perp = \delta\boldsymbol{u}_\perp \pm \delta\boldsymbol{b}_\perp = \hat{\boldsymbol{z}}\times\nabla_\perp\zeta^\pm$.

Equations (4) contain only the perpendicular fluctuations and are, therefore, suitable for simulating Alfvénic turbulence. They are also

more efficient to simulate than MHD, since they involve only two scalar fields. Although originally derived from MHD, it has been shown that RMHD holds for a collisionless plasma such as the solar wind and may, therefore, be more generally applicable (Schekochihin et al. 2009). The RMHD derivation assumes anisotropy ($k_\perp > k_\parallel$) and a strong mean field ($B_0 \gg \delta \boldsymbol{B}_\perp$), both of which are observed at the smallest scales of the solar wind inertial range.

The simulation reported here solves the RMHD equations in a triply periodic cube of size $(2\pi)^3$ with a resolution of 512^3. The Alfvén speed is set to $v_\mathrm{A} = 1$ (making the Alfvén crossing time 2π). It can be seen from equations (4) that if the Alfvén speed is scaled by a factor R and the z coordinate, which is the mean field direction, is also scaled by R, the equations remain identical. This means that a given simulation corresponds to all values of R and therefore to all values of $\delta \boldsymbol{B}_\perp / B_0$ if the box is also stretched in the z direction. The units of length in the perpendicular and parallel directions are independent of each other because the anisotropy is formally infinite and the fluctuation level is infinitely small under the RMHD asymptotic expansion. Different values of R can be chosen, setting the anisotropy and fluctuation level so that the same simulation can be compared to a variety of real-world situations.

The equations are solved pseudo-spectrally in x and y, and using a centred finite difference scheme in z. The time-step is chosen so that the Courant numbers based on both the fluctuation amplitude and the Alfvén speed are much less than unity. With dissipation and forcing terms, the equations are

$$\frac{\partial}{\partial t}\nabla_\perp^2 \zeta^\pm \mp v_\mathrm{A}\frac{\partial}{\partial z}\nabla_\perp^2 \zeta^\pm = -\frac{1}{2}(\{\zeta^+, \nabla_\perp^2 \zeta^-\} + \{\zeta^-, \nabla_\perp^2 \zeta^+\} \mp \nabla_\perp^2\{\zeta^+, \zeta^-\}) + \nu\nabla_\perp^8(\nabla_\perp^2\zeta^\pm) + \nu_z\nabla_z^2(\nabla_\perp^2\zeta^\pm) + f^\pm, \quad (5)$$

where $\nu = 5 \times 10^{-15}$ and $\nu_z = 1 \times 10^{-4}$ are the viscosity coefficients and $f^\pm$ is the forcing term. In the x and y directions, a fourth-order hyperviscosity dissipation term is used, while in the z direction a very small Laplacian viscosity is added to prevent the high k_z modes becoming unstable. Hyperviscosity is used so that the inertial range covers a wide enough range of scales to measure accurate scalings. The magnetic Prandtl number is $\mathrm{Pr_m} = 1$ and the initial conditions are a straight mean field with no fluctuations: $\boldsymbol{b}(\boldsymbol{r}, t = 0) = \hat{\boldsymbol{z}}$ and $\boldsymbol{u}(\boldsymbol{r}, t = 0) = 0$.

The simulation is initially forced on large scales ($k_\perp = 1$, 2 and $k_z = 1$) with Gaussian white noise forcing $f^\pm$, i.e. the random forcing amplitude is refreshed at each time-step. This means that the input power can be controlled; it is set to unity in the code units to produce strong turbulence. We choose to force only the velocity to match possible sources of solar wind forcing, such as velocity shears or large-scale Alfvén waves, so $f^+ = f^-$ at all times. We do not force the magnetic field since there is no known mechanism of breaking magnetic flux conservation at large scales. After a while, the forcing is removed and the simulation is left to freely decay.

A time series of various simulation parameters is shown in Fig. 4. After the simulation begins, the values take a few time units to settle down, which is roughly the turnover time of the largest eddies. The transition between the forced and decaying periods of the simulation can be seen by the change in behaviour of all the quantities at $t = 28$, marked by the dashed line. The top two panels show the rms values of the Elsasser variables, velocity and magnetic field. Their values up to $t = 28$ are determined by the forcing power and after $t = 28$ by the decay of the turbulence. One notable feature is the oscillation in the velocity and magnetic field rms values with a period $\approx 2\pi$. This is most likely due to large-scale Alfvén waves, also seen by Bigot, Galtier & Politano (2008), which should not significantly affect the average inertial range measurements.

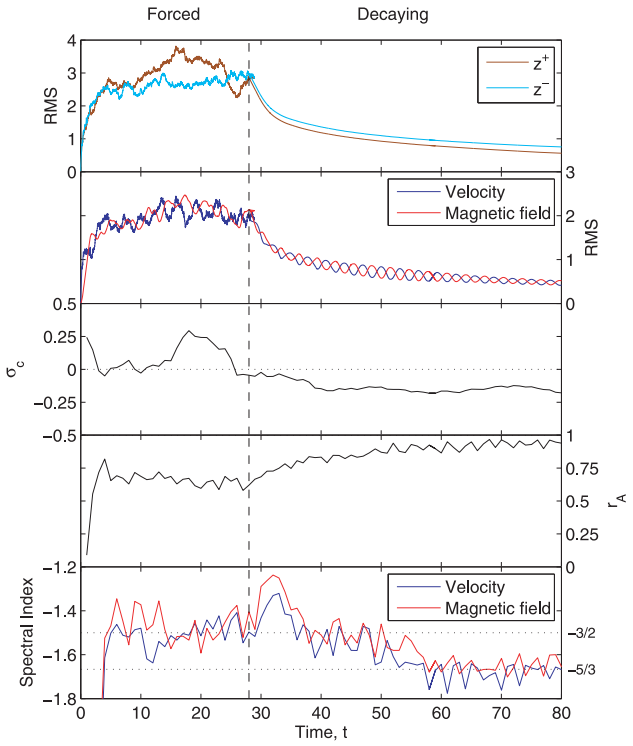

Figure 4. Time series of simulation parameters: rms variables, normalized cross helicity σ_c, Alfvén ratio r_A and Fourier perpendicular spectral indices. For $t \leq 28$ the simulation is forced and for $t > 28$ it is decaying. Spectral index values of $-3/2$ and $-5/3$ are marked as dotted lines for reference in the lower panel.

The normalized cross helicity σ_c in the third panel is calculated spectrally (equation 1), as was done for the solar wind intervals in Section 2.1, and averaged over the range $7 \leq k_\perp \leq 33$. During the forced period, σ_c fluctuates above and below 0. When the forcing is removed, $|\sigma_\mathrm{c}|$ increases, as expected from dynamic alignment theory (Dobrowolny, Mangeney & Veltri 1980). The increase is fairly slow: $|\sigma_\mathrm{c}|$ changes from 0.045 at $t = 28$ to 0.13 at $t = 78$, which is consistent with previous decaying simulations (e.g. Grappin et al. 1982; Matthaeus, Montgomery & Goldstein 1983; Pouquet, Frisch & Meneguzzi 1986; Oughton et al. 1994).

The Alfvén ratio r_A is shown in the fourth panel, calculated over the same range as σ_c. During the forced period $4 \leq t \leq 28$, its mean value is $r_\mathrm{A} \approx 0.66$, which is close to the solar wind observations (Table 1). As the turbulence decays, r_A grows and approaches unity; this equipartition of energy is expected for MHD turbulence (Kraichnan 1965). We note that the opposite effect is seen in simulations without a strong mean field (e.g. Oughton et al. 1994; Biskamp & Müller 1999), in which the Alfvén ratio decreases away from unity as the energy decays. The fact that the equipartition occurs only in the decaying period of our RMHD simulation, while solar wind observations show $r_\mathrm{A} < 1$ (e.g. Matthaeus & Goldstein 1982; Marsch & Tu 1990; Bruno et al. 2007; Podesta et al. 2007; Salem et al. 2009), suggests that solar wind turbulence may be better described by a forced model.

The perpendicular spectral indices for the velocity and magnetic field are shown in the lower panel of Fig. 4. They are calculated from the gradients of the best-fitting lines to the perpendicular energy spectrum in log–log space over the range $7 \leq k_\perp \leq 33$ every time

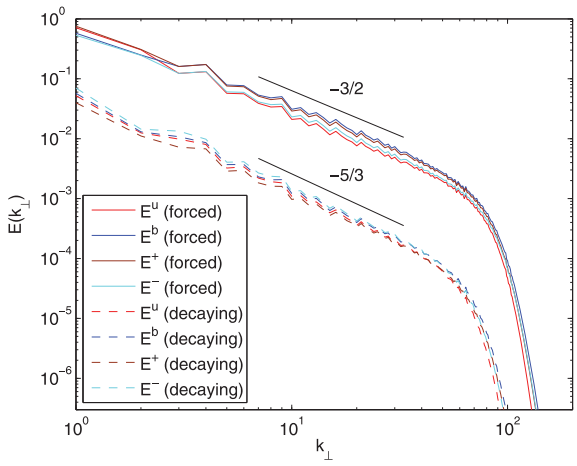

Figure 5. Perpendicular energy spectra of velocity (E^u), magnetic field (E^b) and Elsasser variables ($E^{\pm}$) in the forced and decaying periods of the simulation. Slopes of $-5/3$ and $-3/2$ are given for reference.

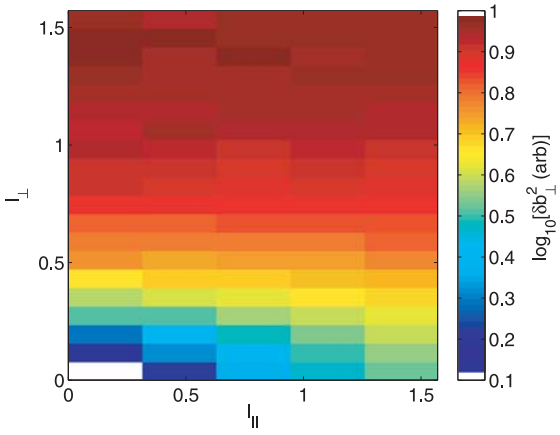

Figure 6. Second-order structure function of the perpendicular magnetic field component for one of the snapshots ($t = 28$) in the forced simulation as a function of parallel ($l_\parallel$) and perpendicular ($l_\perp$) separation.

unit. The perpendicular spectrum is calculated as the sum of the energy in modes nearest to $k_\perp = \sqrt{k_x^2 + k_y^2}$ for integer values of $k_\perp$. During the forced period, the spectral indices are closer to $-3/2$ than $-5/3$, in agreement with previous results (Maron & Goldreich 2001; Müller et al. 2003; Müller & Grappin 2005; Mason et al. 2008; Perez & Boldyrev 2008; Grappin & Müller 2010). When the forcing is removed, however, they gradually steepen and appear to reach a steady value of $-5/3$ from $t = 58$ onwards.

In the following analysis, we investigate the anisotropic scaling in the forced period $4 \leq t \leq 28$ and the decaying period $58 \leq t \leq 78$. We assume that in each of these periods the turbulence is stationary and we can perform time averages over them. The averaged energy spectra are shown in Fig. 5. Before averaging, the decaying spectra are normalized so that the average energy over the range $7 \leq k_\perp \leq 33$ for each is the same as that at $t = 58$. Gradients of $-5/3$ and $-3/2$ are given for reference, although it is hard to tell the difference between these visually. It can be seen that for $7 \leq k_\perp \leq 33$ there are well-defined power laws in all of the spectra. It has been suggested (e.g. Perez & Boldyrev 2010) that the use of hyperviscosity may increase the bottleneck effect, altering the scaling. The spectra in Fig. 5 do not, however, display the increase of energy at small scales that is associated with the bottleneck effect and is seen in some MHD simulations (e.g. Cho & Vishniac 2000; Beresnyak 2011). In the next section, we measure the anisotropic scaling using structure functions, which are expected to be less susceptible to the bottleneck effect than Fourier spectra (Dobler et al. 2003).

3.2 Analysis technique

The technique we use to analyse the simulation data is similar to that used in Section 2.2, with modifications to account for the simulation geometry. First, the scaling factor R, which should be larger than unity for the RMHD equations to be valid, is chosen. Here, we set $R = 4$, which is a compromise between typical solar wind wavevector anisotropies $k_\perp/k_\parallel$ of between 2 and 3 and typical $\delta \boldsymbol{B}_\perp / B_0$ values of 0.1 (calculated from the data in Section 2.3). This means that the simulation, which was solved in a $(2\pi)^3$ box, is now stretched to have a size $(2\pi)^2 \times 8\pi$ and the Alfvén speed is set to 4.

For a particular snapshot in time, many pairs of points in the simulation box are picked at random. The second-order structure function values of the local perpendicular velocity and magnetic field components are calculated and binned, as in Section 2.2. The structure function of the magnetic field binned with respect to $l_\parallel$ and $l_\perp$ at $t = 28$ is shown in Fig. 6. There are on average 10^4 structure function values in each bin. The structure function in Fig. 6 is representative of the general shape of the velocity and magnetic field structure functions in both the forced and decaying periods of the simulation. Similar to the solar wind (Fig. 2) and previous simulations (Cho & Vishniac 2000), the contours are elongated in the parallel direction.

In the range $0.35 \leq l \leq 1.3$, which corresponds approximately to $5 \leq k \leq 18$, the structure functions are approximately power laws and we assume this to be the inertial range of the simulation. The spectral indices and the power anisotropy (calculated at $l = 0.8$) are found from the best-fitting lines to the data binned with respect to l and θ_B in this range. This is done for snapshots separated by 2 time units, giving 13 snapshots for the forced period and 11 for the decaying period.

3.3 Power and spectral index anisotropy

The power and spectral index anisotropy for the velocity and magnetic field are shown in Fig. 7. The error bars are the standard error of the mean from averaging the results of the snapshots in each period. In both cases, the power increases with angle to the local magnetic field θ_B, as it does in the solar wind. For the forced case, the overall power in the magnetic field is larger than that in the velocity, whereas in the decaying case they are similar. This is consistent with our previous discussion of the Alfvén ratio being $r_A < 1$ in the forced case and $r_A \approx 1$ in the decaying case. It is also interesting to note that these curves are qualitatively similar in shape. No prediction for this shape has yet been made based on critical balance theory.

In the forced case, there is a difference between the spectral indices of the velocity and magnetic field. The velocity spectral index varies from -2 at small θ_B to $-5/3$ at θ_B close to 90°. The magnetic field spectral index is also -2 at small θ_B but is less steep at larger θ_B, having a value close to $-3/2$. The fact that both are steep at small angles shows that the turbulence is anisotropic and the -2 scaling is consistent with the critical balance theories of both Goldreich & Sridhar (1995) and Boldyrev (2006). The difference at large angles, however, is unexpected, since theories of Alfvénic turbulence predict that both fields scale in the same way.

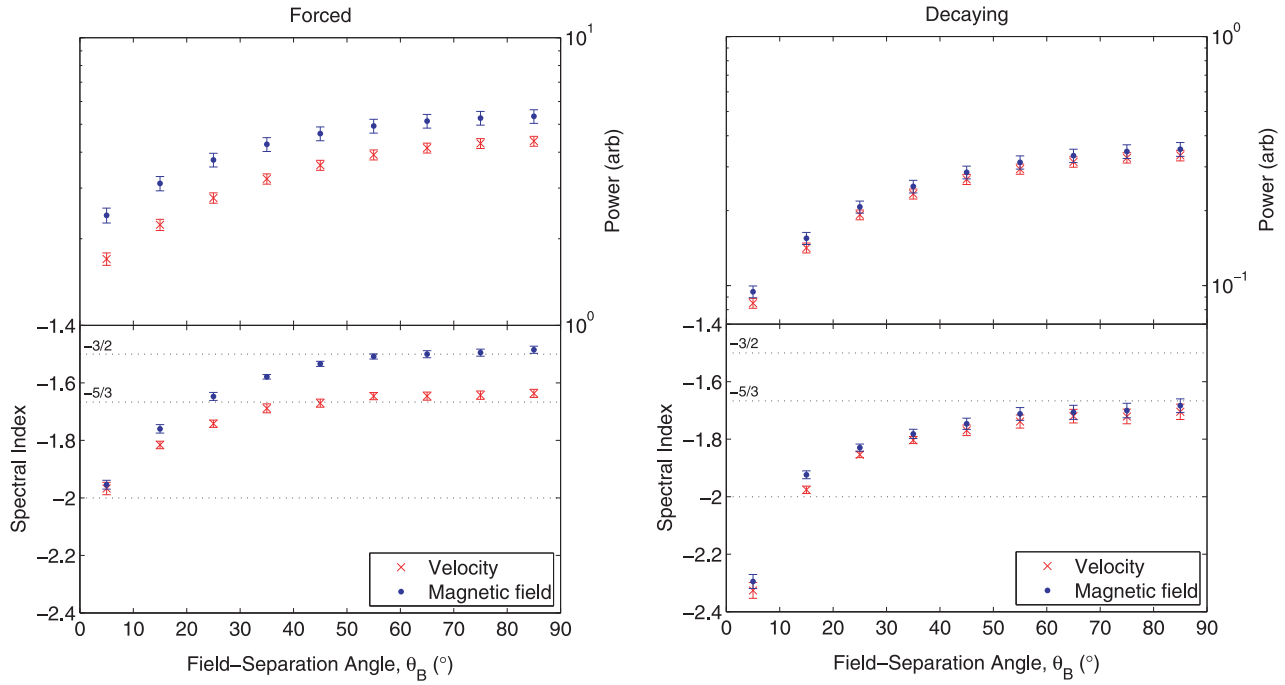

Figure 7. Power anisotropy (upper panels) and spectral index anisotropy (lower panels) of the velocity and magnetic field in the forced (left) and decaying (right) simulations. The power anisotropy is calculated at $l = 0.8$. Spectral index values of $-3/2$, $-5/3$ and -2 are marked as dotted lines for reference.

For the decaying case, both fields show similar scaling. The spectral index is close to $-5/3$ for θ_B close to 90° and much steeper at small θ_B: -2.33 ± 0.03 for velocity and -2.30 ± 0.03 for the magnetic field. Again, the steepening at low θ_B shows the turbulence is anisotropic, although the spectra are steeper than the critical balance prediction of -2. One possible explanation for the steep parallel scaling is that the turbulence may be transitioning to the weak regime, in which there is not thought to be a parallel cascade (Goldreich & Sridhar 1997; Galtier et al. 2000). Perez & Boldyrev (2008) observed the perpendicular spectral index steepening as the turbulence became weaker, and we may be observing a similar effect for the parallel index. In a different run (not shown here) that was forced less strongly, we observed overall steeper spectral indices at all angles. The perpendicular spectral index, however, seems to remain at $-5/3$ for many turnover times in the run here (Fig. 4), rather than dropping to -2 as expected for weak turbulence.

We now compare the spectral indices obtained through the structure function technique to the Fourier indices. The time series of the global perpendicular Fourier indices are shown in the lower panel of Fig. 4. It can be seen that both fields have spectral indices close to $-3/2$ during the forced period and then after a transition reach a value of $-5/3$ in the decaying period. The mean values are -1.51 ± 0.01 for the velocity and -1.47 ± 0.01 for the magnetic field in the forced period and -1.69 ± 0.01 for the velocity and -1.653 ± 0.007 for the magnetic field in the decaying period. These are consistent with the perpendicular spectral indices measured using structure functions, except for velocity in the forced period, which is close to $-5/3$. It is possible that this difference is caused by the forcing, which is localized at large scales in Fourier space, but may affect the structure function, which mixes small- and large-scale information (Davidson & Pearson 2005).

The results we obtain here are broadly consistent with previous simulations. Wavevector anisotropy of the form $k_\perp > k_\parallel$ has been observed previously (e.g. Shebalin et al. 1983; Oughton et al. 1994; Matthaeus et al. 1996; Milano et al. 2001). In particular, Cho & Vishniac (2000) observed a difference in anisotropic scaling between the velocity and magnetic field in their forced simulations. When the mean field was of a similar strength to the rms fluctuations, they obtained $k_\parallel \sim k_\perp^{0.7}$ for velocity but $k_\parallel \sim k_\perp^{0.5}$ for the magnetic field.

We now compare the simulation and solar wind results. First we note that both sets of results are qualitatively similar. Power at a fixed scale is anisotropic and increases as θ_B increases. All spectral index curves are anisotropic and steepen at small θ_B as predicted by critical balance theories. The main difference between the solar wind and simulations is the value of the perpendicular spectral index. For the magnetic field, we observe $-5/3$ in the solar wind and the decaying simulation but $-3/2$ in the forced simulation. Values close to both $-5/3$ and $-3/2$ have been observed previously in the solar wind (Horbury et al. 2008; Podesta 2009; Luo & Wu 2010; Wicks et al. 2010, 2011). In both our forced and decaying simulations, the velocity has a perpendicular spectral index of $-5/3$. Solar wind measurements, however, suggest that it is closer to $-3/2$ (Mangeney et al. 2001; Podesta et al. 2007; Salem et al. 2009; Tessein et al. 2009; Wicks et al. 2011). These differences in perpendicular spectral index remain an unsolved problem.

4 LOCAL VERSUS GLOBAL MEAN FIELD

In this section, we investigate the difference between using the local and global mean magnetic field to define the parallel and perpendicular directions. Fig. 8 shows the spectral index anisotropy for the solar wind magnetic field in the upper panel, the forced simulation magnetic field in the central panel and the forced simulation velocity in the lower panel. In each case, the results obtained using the local mean field are shown in green and those obtained using the global mean in orange. In the solar wind, the global mean field results are obtained by binning the structure function values according to their separation direction with respect to the average field of each

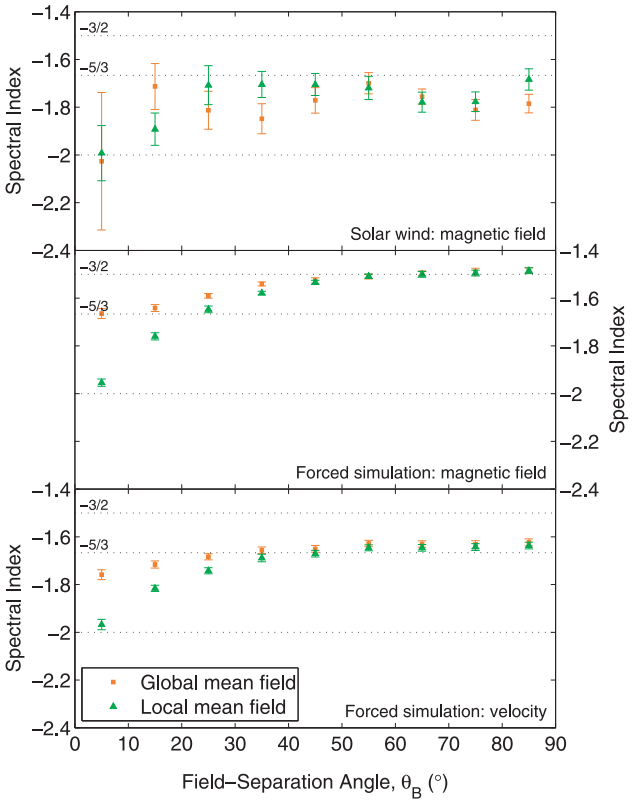

Figure 8. Spectral index anisotropy of magnetic field in the solar wind (upper), magnetic field in the forced simulation (centre) and velocity in the forced simulation (lower) using the local and global mean field methods. Spectral index values of $-3/2$, $-5/3$ and -2 are marked as dotted lines for reference.

interval. In the simulation, they are obtained by binning with respect to the average field over the whole simulation box (the z direction).

In the solar wind, the results are similar for both local and global mean field methods, except for the error bar on the parallel scaling ($0^\circ < \theta_B < 10^\circ$). The error is larger in the global mean field case, which is partly due to the fact that there are fewer intervals where the global mean field is parallel to any separation vectors. This scaling, therefore, is less reliable and the error bar indicates that the data are marginally consistent with an isotropic spectral index with respect to the global mean field. To within errors, these results are not inconsistent with those of Tessein et al. (2009), which show that the spectral index is isotropic when measured with respect to the global mean field.

In the forced simulation, it can be seen that when measured with respect to the global mean field, the spectral indices of both the magnetic field and velocity are much less anisotropic than when they are measured with respect to the local mean field, e.g. in the velocity at small θ_B the spectral index is -1.76 ± 0.02 using the global mean field compared to -1.97 ± 0.02 using the local mean field. This is because the magnetic field fluctuations are large enough that the local mean field direction seen by an eddy is not the same as the global mean field direction. If the fluctuations are in critical balance, the angle between the local and global mean fields is $\delta \boldsymbol{B}_\perp / B_0 \approx k_\parallel / k_\perp$. This suggests that, when using the global mean field, the parallel scaling cannot be correctly distinguished from the perpendicular scaling, even for small $\delta \boldsymbol{B}_\perp / B_0$, because the angle of measurement to the local mean field needs to be less than $k_\parallel / k_\perp$.

This interpretation is in agreement with previous solar wind studies that have used local and global mean field methods. Those that use the global mean field method do not detect spectral index anisotropy (Sari & Valley 1976; Tessein et al. 2009) and those that use a local mean field method do detect it (Horbury et al. 2008; Podesta 2009; Luo & Wu 2010; Wicks et al. 2010, 2011). A similar situation is also seen in simulations, where scaling anisotropy is detected when a local mean field is used (Cho & Vishniac 2000; Maron & Goldreich 2001) but not when a global mean field is used (Grappin & Müller 2010). Here, we have shown that when keeping all other parameters constant, it is indeed the use of the global or local mean field that determines whether the anisotropic scaling is measured. It seems, therefore, that the Alfvénic fluctuations, both in solar wind turbulence and forced RMHD turbulence simulations, are more sensitive to the local mean field at the scale of the fluctuations than the global large-scale field.

In the decaying simulation (not shown in Fig. 8), the local and global mean field methods are much more similar, with the parallel scaling being steeper than -2 in all cases. One possible reason for this is that the scale separation between the global mean field and the fluctuations is not large, meaning that the global and local mean fields are similar. This, combined with the smaller fluctuation amplitudes in the decaying simulation, could account for the observed behaviour. This could be tested by performing a decaying simulation with a larger inertial range.

5 SUMMARY AND CONCLUSIONS

In this paper, we measure the power and spectral index anisotropy of Alfvénic turbulence in the solar wind and RMHD simulations using second-order structure functions. The analysis technique is essentially the same for both, allowing us to make a direct comparison. In the slow solar wind, we find that the magnetic field power and spectral index are anisotropic with respect to the local magnetic field direction. This anisotropy has now been seen by several different methods in both fast and slow wind. In both forced and decaying simulations we also find that the power and spectral index are anisotropic in both the velocity and magnetic field.

In the solar wind, the perpendicular spectral index of the magnetic field is close to $-5/3$, in agreement with the theory of Goldreich & Sridhar (1995). In the forced simulation, the perpendicular spectral indices are close to $-5/3$ for velocity and $-3/2$ for the magnetic field. We are not aware of any theory that can account for this difference, although it may be caused by the velocity forcing. In the decaying simulation, the perpendicular spectral index is close to $-5/3$ for both the velocity and magnetic field. In all cases, the spectral index steepens at small angles to the magnetic field. The parallel scaling obtained in the solar wind and forced simulations is close to -2, which agrees with the theories based on critical balance of both Goldreich & Sridhar (1995) and Boldyrev (2006). The parallel spectral indices in the decaying simulation are -2.33 ± 0.03 for the velocity and -2.30 ± 0.03 for the magnetic field, which are steeper than the critical balance predictions.

We also find that when measuring the anisotropy of the fluctuations in the forced simulation with respect to the global magnetic field, rather than the local mean field, the spectral indices are much less anisotropic. This is expected for critically balanced turbulence and is also consistent with previous solar wind and simulation results: those that used the local mean field saw anisotropic scaling and those that used the global mean field did not.

ACKNOWLEDGMENTS

This work was supported by STFC and the Leverhulme Trust Network for Magnetized Plasma Turbulence. FGM and CIS data were obtained from the Cluster Active Archive. The simulations were carried out using resources at the Texas Advanced Computing Center. We acknowledge useful discussions with R. Wicks and helpful comments from an anonymous referee.

REFERENCES

Bale S. D., Kellogg P. J., Mozer F. S., Horbury T. S., Reme H., 2005, Phys. Rev. Lett., 94, 215002
Balogh A. et al., 2001, Ann. Geophys., 19, 1207
Belcher J. W., Davis L., 1971, J. Geophys. Res., 76, 3534
Beresnyak A., 2011, Phys. Rev. Lett., 106, 075001
Beresnyak A., Lazarian A., 2008, ApJ, 682, 1070
Beresnyak A., Lazarian A., 2009, ApJ, 702, 1190
Bieber J. W., Wanner W., Matthaeus W. H., 1996, J. Geophys. Res., 101, 2511
Bigot B., Galtier S., Politano H., 2008, Phys. Rev. E, 78, 066301
Biskamp D., Müller W.-C., 1999, Phys. Rev. Lett., 83, 2195
Boldyrev S., 2006, Phys. Rev. Lett., 96, 115002
Bruno R., Carbone V., 2005, Living Rev. Sol. Phys., 2, 4
Bruno R., D'Amicis R., Bavassano B., Carbone V., Sorriso-Valvo L., 2007, Ann. Geophys., 25, 1913
Chandran B. D. G., 2008, ApJ, 685, 646
Chen C. H. K., Horbury T. S., Schekochihin A. A., Wicks R. T., Alexndrova O., Mitchell J., 2010a, Phys. Rev. Lett., 104, 255002
Chen C. H. K., Wicks R. T., Horbury T. S., Schekochihin A. A., 2010b, ApJ, 711, L79
Cho J., Vishniac E. T., 2000, ApJ, 539, 273
Coleman P. J., 1968, ApJ, 153, 371
Crooker N. U., Siscoe G. L., Russell C. T., Smith E. J., 1982, J. Geophys. Res., 87, 2224
Dasso S., Milano L. J., Matthaeus W. H., Smith C. W., 2005, ApJ, 635, L181
Davidson P. A., Pearson B. R., 2005, Phys. Rev. Lett., 95, 214501
Dobler W., Haugen N. E., Yousef T. A., Brandenburg A., 2003, Phys. Rev. E, 68, 026304
Dobrowolny M., Mangeney A., Veltri P., 1980, Phys. Rev. Lett., 45, 144
Escoubet C. P., Fehringer M., Goldstein M., 2001, Ann. Geophys., 19, 1197
Falkovich G., 1994, Phys. Fluids, 6, 1411
Galtier S., 2010, in Maksimovic M., Issautier K., Meyer-Vernet N., Moncuquet M., Pantellini F., eds, AIP Conf. Proc.Vol. 1216, Twelfth International Solar Wind Conference. Am. Inst. Phys., New York, p. 109
Galtier S., Nazarenko S. V., Newell A. C., Pouquet A., 2000, J. Plasma Phys., 63, 447
Goldreich P., Sridhar S., 1995, ApJ, 438, 763
Goldreich P., Sridhar S., 1997, ApJ, 485, 680
Goldstein M. L., Roberts D. A., Matthaeus W. H., 1995, ARA&A, 33, 283
Grappin R., Müller W.-C., 2010, Phys. Rev. E, 82, 026406
Grappin R., Frisch U., Pouquet A., Leorat J., 1982, A&A, 105, 6
Horbury T. S., Balogh A., Forsyth R. J., Smith E. J., 1995, Geophys. Res. Lett., 22, 3405
Horbury T. S., Lucek E. A., Balogh A., McComas D. J., 1998, Geophys. Res. Lett., 25, 4297
Horbury T. S., Forman M. A., Oughton S., 2005, Plasma Phys. Controlled Fusion, 47, B703
Horbury T. S., Forman M., Oughton S., 2008, Phys. Rev. Lett., 101, 175005
Kraichnan R. H., 1965, Phys. Fluids, 8, 1385
Lithwick Y., Goldreich P., Sridhar S., 2007, ApJ, 655, 269
Luo Q. Y., Wu D. J., 2010, ApJ, 714, L138
Mangeney A., Salem C., Veltri P. L., Cecconi B., 2001, in Warmbein B., ed., Sheffield Space Plasma Meeting: Multipoint Measurements versus Theory, ESA SP-492. ESA, Noordwijk, p. 53
Maron J., Goldreich P., 2001, ApJ, 554, 1175
Marsch E., Tu C.-Y., 1990, J. Geophys. Res., 95, 8211
Mason J., Cattaneo F., Boldyrev S., 2006, Phys. Rev. Lett., 97, 255002
Mason J., Cattaneo F., Boldyrev S., 2008, Phys. Rev. E, 77, 036403
Matthaeus W. H., Goldstein M. L., 1982, J. Geophys. Res., 87, 6011
Matthaeus W. H., Montgomery D. C., Goldstein M. L., 1983, Phys. Rev. Lett., 51, 1484
Matthaeus W. H., Goldstein M. L., Roberts D. A., 1990, J. Geophys. Res., 95, 20673
Matthaeus W. H., Ghosh S., Oughton S., Roberts D. A., 1996, J. Geophys. Res., 101, 7619
Milano L. J., Matthaeus W. H., Dmitruk P., Montgomery D. C., 2001, Phys. Plasmas, 8, 2673
Monin A. S., Yaglom A. M., 1975, Statistical Fluid Mechanics, Vol. 2. MIT Press, Cambridge, MA
Müller W.-C., Grappin R., 2005, Phys. Rev. Lett., 95, 114502
Müller W.-C., Biskamp D., Grappin R., 2003, Phys. Rev. E, 67, 066302
Osman K. T., Horbury T. S., 2007, ApJ, 654, L103
Osman K. T., Horbury T. S., 2009, Ann. Geophys., 27, 3019
Oughton S., Priest E. R., Matthaeus W. H., 1994, J. Fluid Mech., 280, 95
Perez J. C., Boldyrev S., 2008, ApJ, 672, L61
Perez J. C., Boldyrev S., 2009, Phys. Rev. Lett., 102, 025003
Perez J. C., Boldyrev S., 2010, Phys. Plasmas, 17, 055903
Podesta J. J., 2009, ApJ, 698, 986
Podesta J. J., Bhattacharjee A., 2010, ApJ, 718, 1151
Podesta J. J., Borovsky J. E., 2010, Phys. Plasmas, 17, 112905
Podesta J. J., Roberts D. A., Goldstein M. L., 2007, ApJ, 664, 543
Podesta J. J., Chandran B. D. G., Bhattacharjee A., Roberts D. A., Goldstein M. L., 2009, J. Geophys. Res., 114, 1107
Pouquet A., Frisch U., Meneguzzi M., 1986, Phys. Rev. A, 33, 4266
Rème H. et al., 2001, Ann. Geophys., 19, 1303
Salem C., Mangeney A., Bale S. D., Veltri P., 2009, ApJ, 702, 537
Sari J. W., Valley G. C., 1976, J. Geophys. Res., 81, 5489
Schekochihin A. A., Cowley S. C., Dorland W., Hammett G. W., Howes G. G., Quataert E., Tatsuno T., 2009, ApJS, 182, 310
Shebalin J. V., Matthaeus W. H., Montgomery D., 1983, J. Plasma Phys., 29, 525
Strauss H. R., 1976, Phys. Fluids, 19, 134
Taylor G. I., 1938, Proc. R. Soc. Lond. Ser. A, 164, 476
Tessein J. A., Smith C. W., MacBride B. T., Matthaeus W. H., Forman M. A., Borovsky J. E., 2009, ApJ, 692, 684
Weygand J. M., Matthaeus W. H., Dasso S., Kivelson M. G., Kistler L. M., Mouikis C., 2009, J. Geophys. Res., 114, 7213
Wicks R. T., Horbury T. S., Chen C. H. K., Schekochihin A. A., 2010, MNRAS, 407, L31
Wicks R. T., Horbury T. S., Chen C. H. K., Schekochihin A. A., 2011, Phys. Rev. Lett., 106, 045001

This paper has been typeset from a TEX/LATEX file prepared by the author.